EARTH OBSERVATION AND GEOMATICS ENGINEERING
website: https://eoge.ut.ac.ir

Using GIS and DANP in detecting potential areas for Sinkholes

Hadi Fadaei*[1], Saeideh Sahebi Vayghan[2], Rouhollah Esmaili Sarteshnizi[3] and Neda Ghasemkhani[4]

[1] Ph.D. in remote sensing of natural resources, Department of Geography, Amin Police-Science University, Tehran, Iran
[2] Department of Remote Sensing and GIS, Kharazmi University, Tehran, Iran
[3] Department of Surveing engineering, Marand technical College, University of Tabriz, Tabriz, Iran
[4] Department of Geography and Urban Planning, Islamic Azad University, Tehran, Iran

Article history:
Received: 19 March 2020, Received in revised form: 10 August 2020, Accepted: 15 August 2020

ABSTRACT

One of the most common surface features of Karst topography is sinkholes. The karst areas provide drinking water for 25% of the world's population. Identifying sinkholes is crucial in managing water resources, as their contamination leads to the contamination of water resources in the area. The Bisotun-Parav Karstic Basin is essential because it creates spring wells in Bisotun and Kermanshah and supplies part of their water. This study aims to detect potential areas for sinkholes using GIS and Decision Making Trial and Evaluation Laboratory)-based analytic network process (DANP). The criteria which were used are Climatology (precipitation, temperature, evaporation, streams), Topography (slope, elevation), Agriculture (vegetation), and Lithology (lithology, soil type, fault). Then the required layers were obtained, and the importance of each factor was determined through a combination of the DEMATEL technique and the ANP. Finally, after combining the layers, a map of potential sinkhole areas was obtained. Sinkholes in the area were detected using the visual interpretation of world imagery and google earth imagery as reference data. The results of the DANP demonstrated vegetation, elevation, and lithology with the value of 22.59%, 12.12%, and 11.94 respectively are the most important factors involved in the formation of sinkholes. The indexes of correctness, completeness, and quality were then used to evaluate the study results and turned out to be 98.73%, 79.86%, and 79%, respectively. The high correctness index indicates high efficacy in detecting the existing sinkholes, but the low percentage of the other two indexes does not indicate the inefficacy of the method; rather, the two indexes of completeness and quality indicate areas with a potential for sinkhole formation that either has no sinkholes or are not in the reference data. This method effectively detects sinkholes and potential areas for sinkhole formation.

KEYWORDS
Karst
Sinkhole
Geomorphology
DEMATEL-based
ANP (DANP)
World Imagery

1. Introduction

Sinkholes are common, naturally occurring geologic features, specific to karst areas with carbonate and halite rocks, that are pits formed on the earth's surface and created by the dissolution of limestone (Rosdi, Othman, Abdul, & Yusoff, 2017; Zeng & Zhou, 2019). Karst morphology has major effects on evaluating the vulnerability of karst aquifers. The local catchment area for each sink is proportional to the amount of water infiltrating and the

* Corresponding author
E-mail addresses: fadaei.hd@gmail.com (F.Fadaei); std_saiedehsahebi@khu.ac.ir (s. Sahebi Vayghan); Rouhollahesmaili77@gmail.com (R.Esmaili Sarteshnizi; neda.ghasemkhani@srbiau.ac.ir (N.Ghasemkhani)
DOI: 10.22059/eoge.2021.310615.1090

diameter of the karst conduit (Plan, Decker, & Faber, 2003). The most common surface feature of Karst topography is sinkholes. One of the most common surface features of Karst topography is sinkholes. These features are delineated as or overall refer to a zone of localized land surface subsidence or collapse, through Karst processes, which result in a closed hollow of moderated dimensions (Beck, 1984). There are several types of sinkholes, including dissolution sinkholes, collapse sinkholes, caprock sinkholes, dropout sinkholes, suffusion sinkholes, and buried sinkholes. Sinkhole formation is a major risk factor that can cause significant economic and social damage (Rosa et al., 2018).

It is essential for human sustainability in the karst area to efficiently detect and analyze natural sinkholes (H. Chen, Oguchi, & Wu, 2018). The karst areas provide drinking water for 25% of the world's population (Z. Chen et al., 2017).

Naturally, developing new sinkholes due to the accelerated development of ground-water and land resources makes significant property damage and structural problems for buildings and roads (Tihansky, 1999). Water and environmental resources have been threatened because of sinkholes through draining streams, lakes, wetlands and creating pathways for transmitting surface waters into underlying aquifers (Tihansky, 1999). Transmitting surface contaminants into the underground aquifer systems can persistently degrade ground-water resources due to the development of pathways (Tihansky, 1999). In some zones, sinkholes are utilized as storm rains, and due to their direct link with the underlying aquifer systems, it is substantial their drainage areas be kept free of contaminants. Nonetheless, plugging of sinkholes are leads to flood because of capturing surface-water flow that makes new wetlands, ponds, and lakes (Tihansky, 1999). The sinkholes are closed cavities with internal drainage that are typically associated with the karstic environment to which they are exposed. Soluble rocks can be dissolved by the circulation of surface and groundwater (dissolution sinkholes), but there are other types of sinkholes as well (Rosa et al., 2018). Sinkholes can create in various ways. Dissolution of bedrock by percolated surface water is the most important factor which causes a majority of sinkholes (Launspach, 2013). Piping, collapsing and subsidence can all contribute to the characteristics of the sinkholes (Jennings, 1985). Dissolution of the rock through a chemical reaction permits the rock to dissolve and be released into solution. Over time, conduit forms that are created by dissolving limestone connect surface water to groundwater or caves (Launspach, 2013).

The moving of rainwater through the soil makes it acidic because of dissolving CO2 (Launspach 2013). In addition, Carbonate molecules disassociated by produced carbonic acid (Launspach, 2013):

$$CaCO3 + H2O + CO2 (dissolved) \leftrightarrow Ca+2 + 2HCO3-$$

Piping, collapsing and subsidence can all contribute to the characteristics of the sinkholes (Jennings, 1985). Dissolution of the rock through a chemical reaction permits the rock to dissolve and be released into solution. Over time, conduit forms that are created by dissolving limestone connect surface water to groundwater or caves.

Types of sinkholes indicate that there are general zoning that is controlled by the hydrogeological performance of the various sections: (1)solution sinkholes(polygonal karst) in the high recharge zone; (2)Bedrock collapse sinkholes are located at the lower denudation surface and close to the base surface, where well-developed caves are; and (3)cover subsidence sinkholes, with high densities possibly associated with preferential groundwater discharge areas (Gökkaya, Gutiérrez, Ferk, & Görüm, 2021).

one of the most hazardous elements in mantled karst environments is cover-collapse sinkholes(Jia, Meng, Li, & Yin, 2021). Long Jia et al., in 2021 want to establish a methodological framework using different techniques and approaches to understand cover-collapse sinkhole and its possible evolution. During their studies, titled "A multidisciplinary approach in cover-collapse sinkhole analyses in the mantle karst from Guangzhou City (SE China)", morphometry, the detailed typology and morphometry and chronology inventory of 49 cover-collapse sinkholes have been analyzed and three karst fissure zones covered by Quaternary soils were found. In their research, hydrogeological data indicate that karstic aquifer pumping causes a decrease in groundwater level. Cover-collapse sinkholes may be attributed to soil erosion due to declining groundwater levels (Jia et al., 2021).

When carbonate substrates are under non-carbonate formations, the seismic changes caused by faults may compress the aquifers of the area and move them upward, leading to erosion and collapse (Harrison, Newell, Necdet, & Kuniansky, 2002; Wadas, Tanner, Polom, & Krawczyk, 2017). There are two types of sinkholes, natural and human-made. Natural sinkholes are mainly found in areas with great deposits of salt, limestone, and carbonate. It is very important, though difficult, to accurately predict the location and timing of these sinkholes (Ali & Choi, 2019). Effective discovery and analysis of natural basins are essential for human sustainability in the karstic area (H. Chen et al., 2018).

Despite the hazards caused by sinkholes (such as groundwater pollution, sudden subsidence of residential areas, land degradation), karstic landscapes have a variety of economic, scientific, educational, recreational, and aesthetic values. On the other hand, these areas are highly sensitive and it is essential to manage their protection. Karstic areas have several values that can be summarized in three groups: scientific, human, and economic value (Khoshakhlagh, BAGHERI, & Safarrad, 2015). Karstic areas also supply potable water to 25 percent of the world's population (D.

Ford & Williams, 2013; Milanovic, 1981). Sinkholes are one of the most important morphological indicators that play a crucial role in water absorption, water penetration into the earth, feeding and discharging the karstic aquifers, and human concerns such as agriculture and population attraction, and so on.

So far, several studies have been conducted in the field of karst in different places. One of the first leading researchers in this field was Jovan Cvijic (D. C. Ford & Williams, 1989). He is now known as the founder of karst due to his comprehensive research on karst (Harmon, Wicks, Ford, & White, 2006). There have been many field-based studies on sinkholes in such areas as formation mechanisms (Salvati & Sasowsky, 2002; Tharp, 1999), terminology and classification (Gunn, 2004; Gutiérrez, Guerrero, & Lucha, 2008; Waltham, Waltham, Bell, & Culshaw, 2005; White, 1998), interaction with the human environment (Gutiérrez, Parise, De Waele, & Jourde, 2014; Rose, Federico, & Parise, 2004) and risk assessment (Taheri, Gutiérrez, Mohseni, Raeisi, & Taheri, 2015; Van Schoor, 2002). Various methods for karst sinkhole recognition have been done include using a similar sink-filling method of processing LiDAR data to map sinkholes (Zhu, Taylor, Currens, & Crawford, 2014), image filtering techniques with kernel windows using focal functions (Obu & Podobnikar, 2013), using an algorithm that delineates sinkhole boundaries based on changes in flow of the elevation gradient (Rahimi & Alexander Jr, 2013), (applying a sink-filling method on LiDAR data to create a depression-less Digital Elevation Model (DEM), substracting the layer from the depressionless/filled DEM layer and processing it with different thresholds of elevation differences to locate sinkholes (Mukherjee & Zachos, 2012). Karst areas play an important role in the lives of residents and are especially important in providing water resources, especially in arid and semi-arid countries (Behniafar, Ghanbarzadeh, & FARZANEH, 2009) . In 2014, Sarvati et al. investigated the factors controlling sinkhole besides their morphometry, which demonstrated that no sinkholes were observed on a slope above 20°. Also, based on the result of logistic analysis, they showed that the most important variables in the occurrence of sinkholes are fault, height and precipitation, respectively (Sarvati, Rostami, Nosrati, & Ahmadi, 2014). In 2004, Amiri et al., in a study conducted in the Famenin Kaboudar Ahang plain located in the north of Hamadan province, concluded that during the past ten years, at least 19 small and large sinkholes have been occurred on the plain, which tthe existence of the holes, water canals, joints and fracture systems in the limy bed rock and the pumping of water from wells, are the main caused of forming the sinkholes. Plus, some other factors including sand washing of layers gas leakage from the wells and rapid decline of groundwater level, accelerate such a process (Amiri, Mazaheri, & Nazaripoya, 2004).

However, it is still a challenge to accurately detect sinkholes at a small size. In the past, it was customary to detect sinkholes based on visual interpretation of remote sensing images and fieldwork, which was both time-consuming and inaccurate (Doctor & Young, 2013). The present study, however, uses GIS and the DANP method to investigate and evaluate the detection of sinkholes and the parameters involved in their formation.

2. The Proposed Method

The study area is a part of the Zagros overthrust, which is located in Kermanshah province and northeast of Kermanshah city in Figure 1. It has an approximate length of 40 km and a maximum width of 15 km, and in accordance with the location of the main Zagros fault, it is in the northwest-southeast direction. This mass is located between latitudes 21°34′ to 34°44′ north and longitudes 53°46′ to 27°47′ east. The Bisotun Wall, the largest fault wall in the Zagros overthrust, is located on the southern slope of these terrains (Maghsoudi, Karimi, Safari, & Charrahi, 2010). The climate of the region changes a great deal throughout the year in terms of temperature and precipitation and the study area is located in the Zagros orogenic belt (Alavi, 1994). The Bisotun subzone is located in the northeast of the radiolarite subzones, formerly known as the internal carbonate continent platform(Kazmin et al. 1986).

The present study considers ten criteria (precipitation, temperature, evaporation, lithology, soil type, slope, height, fault, streams, and vegetation) to determine the potential areas for sinkhole formation. In this study expert's opinions have been used to determine the criteria and identify the relations between them. Moreover, the DEMATEL technique has been used to provide the structure. The structure was obtained through a questionnaire completed by experts. Furthermore, the Decision Making Trial and Evaluation Laboratory (DEMATEL) technique builds an influential relationship among dimensions and criteria, DANP to find the significant weights. The weighted layers were then overlaid and analyzed by the geographic information system and finally matched with the sinkholes extracted from the World Imagery and Google Earth images to calculate the indexes of correctness, accuracy, and quality.

2.1. Analytic Network Process (ANP)

Analytic Network Process (ANP) as a generalized form of Analytic Hierarchy Process (AHP) is one of the MCDM approaches widely utilized to resolve different problems due to the consideration of complicated and interrelated relationships between decision factors and the ability to

apply quantitative and qualitative attributes simultaneously. In the ANP method, considering the relationship between criteria is possible in addition to the hierarchical structure (Kheybari, Rezaie, & Farazmand, 2020). Moreover, ANP consists of a binary comparison similar to that in the AHP method. ANP computes complex relationships between decision elements through the replacement of a hierarchical structure with a network structure (Saaty, 1999). ANP has all the positive features of AHP, including simplicity, flexibility, simultaneous use of quantitative and qualitative criteria, and the ability to review consistency in judgments. ANP considers each issue as a network of criteria, sub-criteria, and alternatives. All elements in a network can communicate with each other in any way. In other words, in a network, feedback and interconnection are possible between clusters (García-Melón, Ferrís-Oñate, Aznar-Bellver, Aragonés-Beltrán, & Poveda-Bautista, 2008). The decision elements in each of the clusters are compared pairwise according to their importance in relation to the control criteria. Decision-makers have to make pairwise comparisons of the criteria and then the subcriteria. The relative importance of the elements is measured on the basis of a 9-variable Saaty scale (the AHP scale). In this section, the vector of internal importance is calculated, which indicates the relative importance of the elements or clusters. It is obtained through the following Eq. (1).

$$Aw = \lambda_{max} w \quad (1)$$

In this equation, A is the matrix of binary comparison of the criteria, W the special vector (significance coefficient), and λ_{max} is the largest special numerical value (Zebardast, 2010). Thus, in this step, the internal priority vectors are calculated. The questionnaire used for the hierarchical analysis and the multivariate decision-making is called the expert questionnaire.

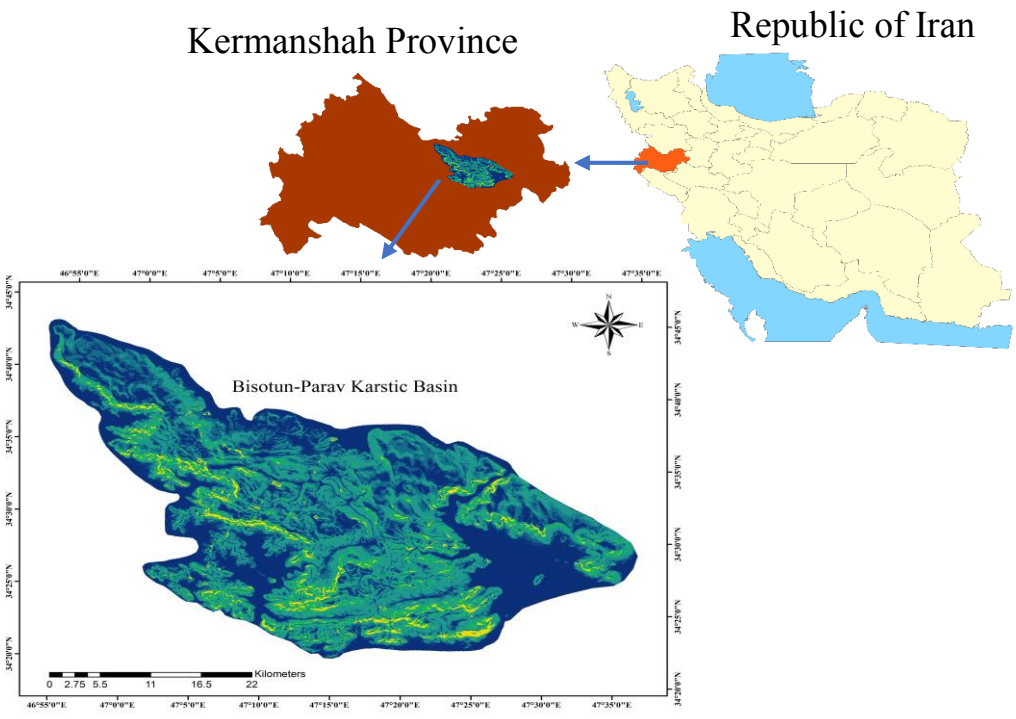

Figure 1. Slope map of the study area

2.2. DANP Technique

In conventional ANP it is assumed that every cluster has a similar weight although it is clear that the effect of one cluster over others can be different. Therefore, the conventional ANP assumption which is about the weight of clusters being the same in making harmonious super-matrixes is not logical. Instead, the effective DANP weights can elevate this deficiency. In this method, the results are calculated based on the ANP concept of total T_c and T_d matrix measured by DEMATEL. Therefore, the DEMATEL technique is used in making network structures for each criterion and dimension in order to improve the conventional ANP normalization process (Chiu, Tzeng, & Li, 2013) Compared to conventional approaches, this technique is very proper in real-world issues, and considers the dependency between criteria and ultimately DEMATEL is combined with ANP in order to make DANP so we can determine the effective weights in every criteria and dimension. The steps in making network structures with the use of the DEMATEL technique and determining the effective DANP weights based on the total communication DANP matrix are shown in Figure 2.

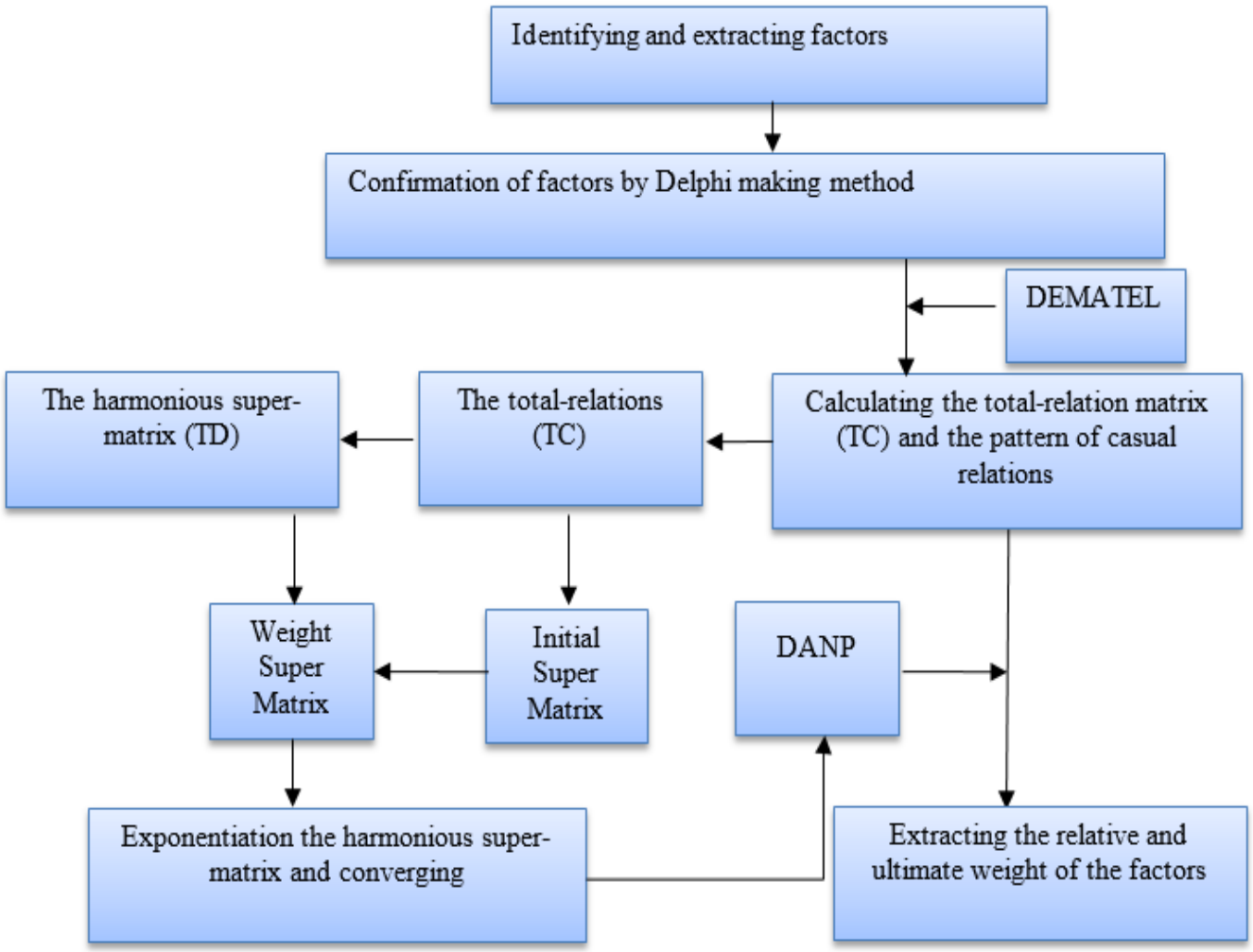

Figure 2. DANP Algorithm

2.3. DEMATEL technique for drawing the map of network relations

First step: calculating the direct relation matrix

Assessing the relation between criteria (the effect of one criterion over the other) is done based on the opinions of the experts of the research from grading range of 0 to 4 in which 0 is the sign of no effect, 1- small effect, 2-average effect, 3-high effect, 4- super-high effect. The experts are asked to determine the effect of one criterion over the other. It means if they believe that the i criteria affected the j criteria they must show it like d_c^{ij}. Therefore, the $D = [d_c^{ij}]$ direct matrix will be drawn (2).

$$D = \begin{bmatrix} d_c^{11} & \dots & d_c^{1j} & \dots & d_c^{1n} \\ \vdots & & \vdots & & \vdots \\ d_c^{i1} & \dots & d_c^{ij} & \dots & d_c^{in} \\ \vdots & & \vdots & & \vdots \\ d_c^{n1} & \dots & d_c^{nj} & \dots & d_c^{nn} \end{bmatrix} \quad (2)$$

The second step: making the direct matrix relation normal

The D matrix direct relation is normalized through the relation below and thus the N matrix is drawn (3).

$$N = VD;\ V = \min_i \{1/max \sum_{j=1}^{n} d_{ij}\ , 1/\ max_j \sum_{i=1}^{n} d_{ij}\}, i,j \in \{1,2,\dots,n\} \quad (3)$$

The third step: when the D matrix is normalized and the N matrix is drawn, the total relations matrix will happen. In this relation, I reflect a single matrix (4).

$$T = N + N^2 + \cdots + N^h = N(I-N)^{-1}, when\ h \to \infty \quad (4)$$

The total relation matrix can be counted with criteria which are shown by T_C(5).

$$T_c = \begin{array}{c} c_{11} \\ c_{12} \\ D_1 c_{1m_1} \\ \vdots \\ \vdots \\ c_{i1} \\ c_{i2} \\ D_i c_{imj} \\ \vdots \\ \vdots \\ c_{n1} \\ D_n \; c_{n2} \\ c_{nmn} \end{array} \overbrace{\begin{array}{ccccc} D_1{}_{c11\ldots c1m1} & \cdots & D_j{}_{cj1\ldots cjm_j} & \cdots & D_n{}_{cn1\ldots cnmn} \\ \left[\begin{array}{ccccc} T_c^{11} & \ldots & T_c^{1j} & \ldots & T_c^{1n} \\ \vdots & & \vdots & & \vdots \\ T_c^{i1} & \ldots & T_c^{ij} & \ldots & T_c^{in} \\ \vdots & & \vdots & & \vdots \\ T_c^{n1} & \ldots & T_c^{nj} & \ldots & T_c^{nn} \end{array}\right] \end{array}} \quad (5)$$

The fourth step: analyzing the results, in this step, the sum of lines and columns of the matrix is calculated completely and separately based on the relation below (6).

$$T = [t_{ij}], i,j \in \{1,2,\ldots,n\}$$
$$r = [r_i]_{n\times 1} = \left[\sum_{j=1}^{n} t_{ij}\right]_{n\times 1} \qquad c = [c_j]_{1\times n} = \left[\sum_{i=1}^{n} t_{ij}\right]_{1\times n} \quad (6)$$

The r_i index shows that the sum of line i and c_j expresses the sum of j column. The $r_i + c_j$ index is the result of the sum of line i and column j (i=j). This index expresses the importance of the i criteria. Similarly, the $r_i - c_j$ index is the result of subtraction addition of line i and column j and shows the effects on and by the i criteria. In general, if $r_i - c_j$ is positive, the criteria i would be in the effective category. If $r_i - c_j$ is negative (i=j), the i criteria would be part of the affected categories. The effecting diagram is drawn based on the two indexes which are also known for the network relations' map. According to this map, it can be decided on how to improve the dimensions and criteria.

2.4. DANP techniques to find effective weights for each factor

The fifth step: normalization of the total relation dimension matrix (T^x_D)

The T_D matrix is drawn from the average of T_C^{ij}. This matrix will be normalized based on the method below, therefore the sum of the three lines and each element will be divided into the related elements of each line. The normalized total relation T_D (7) matrix will be shown like $T_D^{\propto}$ (8).

$$T_D = \begin{bmatrix} t_{11}^{D11} & L & t_{1j}^{D_{1j}} & L & t_m^{D_{1m}} \\ M & M & M & M & M \\ t_{i1}^{D_{t1}} & L & t_{ij}^{D_{ij}} & L & t_{im}^{D_{im}} \\ M & M & M & M & M \\ t_{m1}^{D_{m1}} & L & t_{mj}^{D_{mj}} & L & t_{mm}^{D_{mm}} \end{bmatrix} \begin{array}{l} \to d_1 = \sum_{j=1}^{m} t_{1j}^{D_{ij}} \\ \to d_i = \sum_{j=1}^{m} t_{ij}^{D_{ij}}, d_i = \sum_{j=1}^{m} t_{1j}^{D_{ij}}, i = 1,\ldots,m \\ \to d_m = \sum_{j=1}^{m} t_{mj}^{D_{mj}} \end{array} \quad (7)$$

$$\boldsymbol{T_D^{\propto}} = \begin{bmatrix} t_{11}^{D_A}/d_1 & L & t_{1j}^{D_j}/d_1 & L & t_{1m}^{D_m}/d_1 \\ M & M & M & M & M \\ t_A^{D_A}/d_1 & L & t_{ij}^{D_i}/d_1 & L & t_{1m}^{D_m}/d_1 \\ M & M & M & M & M \\ t_{ij}^{D_A}/d_m & L & t_{ij}^{D_{ij}}/d_m & L & t_{ij}^{D_A}/d_m \end{bmatrix} = \begin{bmatrix} t_D^{\propto 11} & L & t_D^{\propto 1j} & L & t_D^{\propto 1m} \\ M & & M & & M \\ t_D^{\propto 11} & L & t_{cij}^{\propto ij} & L & t_D^{\propto m} \\ M & & M & & M \\ t_D^{\propto 11} & L & t_D^{\propto 11} & L & t_D^{\propto 11} \end{bmatrix} \quad (8)$$

The sixth step: normalization of the total relation criteria matrix ($T_C^{\propto}$) (9)

The T_C normalization with the sum of the impact and influence of the criteria and dimensions in order to gain T^x_C is mentioned below.

$$T_c^{\propto} = \begin{array}{c} c_{11} \\ c_{12} \\ D_1 c_{1m_1} \\ \vdots \\ \vdots \\ c_{i1} \\ c_{i2} \\ D_i c_{imj} \\ \vdots \\ \vdots \\ c_{n1} \\ D_n \; c_{n2} \\ c_{nmn} \end{array} \overbrace{\begin{array}{ccccc} D_1{}_{c11\ldots c1m1} & \cdots & D_j{}_{cj1\ cjm_j} & \cdots & D_n{}_{cn1\ldots cnmn} \\ \left[\begin{array}{ccccc} T_c^{\propto 11} & L & T_c^{\propto 1j} & L & T_c^{\propto 1n} \\ M & & M & & M \\ T_c^{\propto i1} & L & T_c^{\propto ij} & L & T_c^{\propto in} \\ M & & M & & M \\ T_c^{\propto n1} & L & T_c^{\propto nj} & L & T_c^{\propto nn} \end{array}\right] \end{array}} \quad (9)$$

In the following, there is an example of the how-to normalize $T_C^{\propto 11}$ (10) other $T_c^{\propto nm}$ (11) will be calculated the same way.

$$d_{ci}^{11} = \sum_{j=1}^{m_1} t_{cij}^{11} \ , i = 1, 2, \dots, m_1 \qquad (10)$$

$$\boldsymbol{T_C^{\propto 11}} = \begin{bmatrix} t_{c11}^{11}/d_{c1}^{11} & \dots & t_{c1j}^{11}/d_{c1}^{11} & \dots & t_{c1m1}^{11}/d_{c1}^{11} \\ \vdots & & \vdots & & \vdots \\ t_{ci1}^{11}/d_{ci}^{11} & \dots & t_{cij}^{11}/d_{ci}^{11} & \dots & t_{cim1}^{11}/d_{ci}^{11} \\ \vdots & & \vdots & & \vdots \\ t_{cm11}^{11}/d_{cm1}^{11} & \dots & t_{cm1j}^{11}/d_{cm1}^{11} & \dots & t_{cm1m1}^{11}/d_{cm1}^{11} \end{bmatrix} = \begin{bmatrix} t_{c11}^{\propto 11} & \dots & t_{c1j}^{\propto 11} & \dots & t_{c1m1}^{\propto 11} \\ \vdots & & \vdots & & \vdots \\ t_{ci1}^{\propto 11} & \dots & t_{cij}^{\propto 11} & \dots & t_{cim1}^{\propto 11} \\ \vdots & & \vdots & & \vdots \\ t_{cm1\,1}^{\propto 11} & \dots & t_{cm1j}^{\propto 11} & \dots & t_{cm1m1}^{\propto 11} \end{bmatrix} \qquad (11)$$

The seventh step: making the inharmonious W super-matrix. In this step, the transposed total relation matrix T^X_C is calculated and the W matrix is drawn. So as an example, if a matrix-like w^{11} is empty or zero, this means that the matrix is independent (12).

$$W = (T_c^{\propto}) \begin{array}{c} c_{11} \\ c_{12} \\ D_1 c_{1m_1} \\ \vdots \\ \vdots \\ c_{i1} \\ c_{i2} \\ D_i c_{imj} \\ \vdots \\ \vdots \\ c_{n1} \\ D_n \ c_{n2} \\ c_n \quad mn \end{array} \overbrace{\begin{array}{ccccc} D_{1_{c11\dots c1m1}} & \dots & D_{j_{cj1\dots cjmj}} & \dots & D_{n_{cn1\dots cnmn}} \\ \hline W^{11} & L & W^{j1} & L & W^{n1} \\ M & & M & & M \\ W^{1j} & L & W^{ij} & L & W^{nj} \\ M & & M & & M \\ W^{1n} & L & W^{in} & L & W^{nn} \end{array}} \qquad (12)$$

The eighth step: the making of the harmonious super-matrix
In order to make a harmonious super-matrix, the normal total relation matrix $T_D^{\propto}$ will be transposed and multiply into the inharmonious super-matrix (13).

$$\boldsymbol{W^{\propto}} = \boldsymbol{T_D^{\propto} W} = \begin{bmatrix} t_D^{\propto 11} \times W^{11} & \dots & t_D^{1i1} \times W^{i1} & \dots & t_D^{\propto n1} \times W^{n1} \\ \vdots & & \vdots & & \vdots \\ t_D^{\propto 1j} \times W^{1j} & \dots & t_D^{\propto ij} \times W^{ij} & \dots & t_D^{\propto nj} \times W^{nj} \\ \vdots & & \vdots & & \vdots \\ t_D^{\propto 1n} \times W^{1n} & \dots & t_D^{\propto in} \times W^{in} & \dots & t_D^{\propto nn} \times W^{nn} \end{bmatrix} \qquad (13)$$

The ninth step: limiting the harmonious super-matrix
We limit the harmonious super-matrix through the exponentiation of it toward a Z large number. We do it till the super-matrix becomes convergent and stabilized. The outcome of these influential weights will be DANP (14).

$$\lim_{Z \to \infty} (W^{\propto})^Z \qquad (14)$$

2.5. Introducing the research factors

This research has 4 main criteria and 10 sub-criteria which are introduced in Table 1.

Table 1. Introducing the research factors

Criteria	Code	Sub-criteria	Code
Climatology	C	Precipitation	c_1
		Streams	c_2
		Temperature	c_3
		Evaporation	c_4
Topography	T	Elevation	t_1
		Slope	t_2
Agriculture	A	Vegetation	a_1
Geology	G	Lithology	g_1
		Soil type	g_2
		Fault	g_3

2.6. DANP method results

In this step, we form the direct relations matrix in order to measure the relation between the factors (the effect of one factor over the other) with the use of the opinions of the experts of the research which is based on a 0-4 range. In the DANP technique when the research model contains the criteria and sub-criteria, the direct relation matrix will be formed only for the sub-criteria. To check the factors, the opinions of 6 experts so we should average their opinions seriously. The results are shown in Table 2.

2.7. Normalization of the decision matrix

In this step, we normalize the direct relation matrix through relation 7. The results are shown in Table 3. In order to normalize, we must first find the sum of the entry of lines and columns. Then, we choose the biggest number from among them and perform division of each entry over this number. In this research, the biggest number is the sum of lines and columns which is equal to 12.333. Then, we divide all the table 3 entries into this number in order to gain the normalized matrix.

2.8. Calculating the total relation matrix (T_C)

In order to calculate the total relation matrix based on the 3-4 relation, first the Identity Matrix (I_{8*8}) is shaped. Then, we subtract the identity matrix from the normal matrix and we reverse the resulted matrix. Finally, we multiply the normal matrix into the reversed matrix. The total relation matrix is shown in Table 4.

2.9. The affectivity and influence of sub-criteria

In this step, we identify the affectivity and influence of the sub-criteria through relations 10 and 11. The influential sub-

criteria are under the category of cause and the affective criteria are under the category of effect. The results are shown in Table 5. Also, the cause and effect diagram of indexes is drawn in Figure 2.

According to Table 5, the index which has a bigger D is the most influential factor in the system. Therefore, height c_1 (Precipitation) is the most effective factor. Also, the index which has the biggest R is the most effective factor. According to this, the residential, industrial, sports, business, administrative and therapeutic users on sterile user g_1 (Lithology) is the most effective factor in Figure 3.

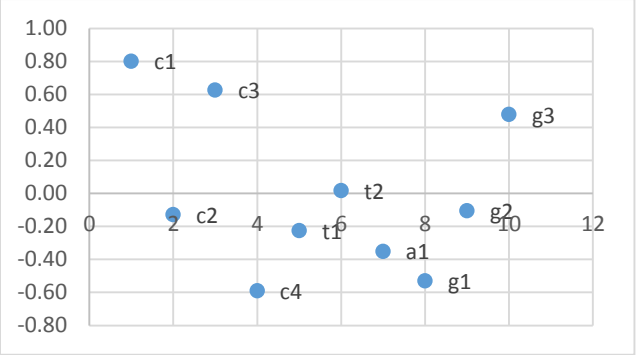

Figure 3. The cause diagram of sub-criteria

Table 2. The direct relation matrix

Criteria		C				T		A	L		
	Sub criteria	c_1	c_2	c_3	c_4	t_1	t_2	a_1	g_1	g_2	g_3
C	c_1	0	3	3	3	0	2	3	4	3	2
	c_2	2	0	2	3	0	1	2	3	2	1
	c_3	3	3	0	2	3	1	2	3	1	1
	c_4	3	2	2	0	0	0	2	1	1	0
T	t_1	3	2	0	2	0	0	0	2	0	0
	t_2	1	1	0	1	3	0	1	2	2	1
A	a_1	1	0	2	1	2	2	0	1	2	0
L	g_1	1	3	2	2	1	2	2	0	3	0
	g_2	1	2	1	2	2	2	1	3	0	1
	g_3	1	1	1	1	2	1	0	2	1	0

Table 3. The normal direct relation matrix

Criteria		C				T		A	L		
	Sub-criteria	c_1	c_2	c_3	c_4	t_1	t_2	a_1	g_1	g_2	g_3
C	c_1	0.00	0.13	0.13	0.13	0.00	0.09	0.13	0.17	0.13	0.09
	c_2	0.09	0.00	0.09	0.13	0.00	0.04	0.09	0.13	0.09	0.04
	c_3	0.13	0.13	0.00	0.09	0.13	0.04	0.09	0.13	0.04	0.04
	c_4	0.13	0.09	0.09	0.00	0.00	0.00	0.09	0.04	0.04	0.00
T	t_1	0.13	0.09	0.00	0.09	0.00	0.00	0.00	0.09	0.00	0.00
	t_2	0.04	0.04	0.00	0.04	0.13	0.00	0.04	0.09	0.09	0.04
A	a_1	0.04	0.00	0.09	0.04	0.09	0.09	0.00	0.04	0.09	0.00
L	g_1	0.04	0.13	0.09	0.09	0.04	0.09	0.09	0.00	0.13	0.00
	g_2	0.04	0.09	0.04	0.09	0.09	0.09	0.04	0.13	0.00	0.04
	g_3	0.04	0.04	0.04	0.04	0.09	0.04	0.00	0.09	0.04	0.00

Table 4. The total relation matrix (T_C)

Criteria		C				T		A	L		
	Sub-criteria	c_1	c_2	c_3	c_4	t_1	t_2	a_1	g_1	g_2	g_3
C	c_1	0.19	0.33	0.29	0.33	0.15	0.23	0.30	0.40	0.32	0.15
	c_2	0.22	0.16	0.21	0.27	0.11	0.15	0.21	0.30	0.22	0.09
	c_3	0.29	0.30	0.15	0.27	0.23	0.16	0.23	0.33	0.21	0.10
	c_4	0.23	0.20	0.19	0.12	0.08	0.08	0.19	0.18	0.15	0.05
T	t_1	0.21	0.18	0.09	0.18	0.05	0.07	0.09	0.20	0.10	0.04
	t_2	0.14	0.15	0.08	0.15	0.19	0.07	0.12	0.21	0.18	0.08
A	a_1	0.14	0.11	0.16	0.14	0.16	0.15	0.08	0.16	0.17	0.04
L	g_1	0.18	0.27	0.20	0.23	0.15	0.18	0.21	0.18	0.26	0.06
	g_2	0.17	0.22	0.15	0.22	0.17	0.17	0.15	0.28	0.13	0.09
	g_3	0.13	0.14	0.12	0.14	0.14	0.10	0.08	0.19	0.13	0.03

Table 5: The affectivity and influence of sub-criteri

Criteria	Sub-criteria	D	R	D + R	D - R	Estate
C	c_1	2.70	1.89	4.59	0.80	Cause
	c_2	1.95	2.07	4.02	-0.13	Effect
	c_3	2.27	1.64	3.91	0.63	Cause
	c_4	1.47	2.06	3.53	-0.59	Effect
T	t_1	1.21	1.43	2.64	-0.22	Effect
	t_2	1.37	1.35	2.73	0.02	Cause
A	a_1	1.32	1.67	2.98	-0.35	Effect
L	g_1	1.91	2.44	4.34	-0.53	Effect
	g_2	1.75	1.85	3.60	-0.10	Effect
	g_3	1.21	0.73	1.93	0.48	Cause

2.10. With the formation of the total relation dimension matrix (T^{x}_{d}) and its normalization in this step, we form the total relations matrix with the use of relation 12. Then through relation 13, we normalize this matrix. In order to normalize, we divide each entry over the sum of each line. Then, we form its transposition. The results are shown in Table 6.

Table 6. Transposition of the normal total relation dimension matrix (T^{X}_{D})

	C	T	A	G
C	0.28	0.18	0.28	0.25
T	0.31	0.19	0.22	0.27
A	0.28	0.31	0.16	0.25
G	0.29	0.24	0.23	0.24

2.11. The formation of the inharmonious super matrix
In this step, we normalize the total relation matrix (Table 5) through relation 14. Then, we transpose it which results in the inharmonious super matrix. The results are shown in Table 7

2.12. The formation of the harmonious super -matrix
In this step, it is enough to multiply the normalized total relation matrix T^{X}_{D} in Table 6
In to inharmonious super matrix (Table 7). The results are shown in Table 8 which is the harmonious super-matrix.

2.13. Limiting the harmonious super matrix
In this step, one must exponentiate the harmonious super-matrix till it is convergent. In this research, the harmonious matrix is converted into 5 exponents are shown in Table 9.

2.14. The influential weights of criteria and sub criteria using DANP

According to the limited super matrix, the weights of criteria (Figure 4) and sub-criteria (Figure 5) are drawn. The entries of the limited super matrix are the influential weights of the research factors which is shown in Table 10

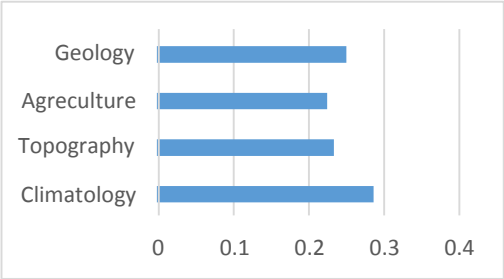

Figure 4. The weight and degree of main criteria

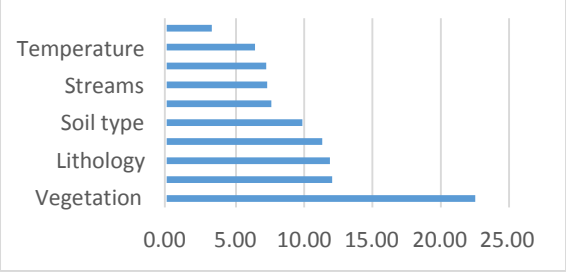

Figure 5. The weight and degree of sub-criteria

Table 7. The inharmonious super-matrix

Criteria		C				T		A	L		
	Sub-criteria	c1	c2	c3	c4	t1	t2	a1	g1	g2	g3
C	c1	0.17	0.26	0.29	0.31	0.31	0.27	0.25	0.20	0.22	0.25
	c2	0.29	0.18	0.30	0.27	0.28	0.29	0.20	0.30	0.29	0.27
	c3	0.26	0.25	0.15	0.25	0.13	0.16	0.29	0.23	0.20	0.22
	c4	0.29	0.32	0.26	0.17	0.28	0.29	0.26	0.26	0.29	0.26
T	t1	0.40	0.42	0.59	0.48	0.43	0.73	0.52	0.45	0.50	0.59
	t2	0.60	0.58	0.41	0.52	0.57	0.27	0.48	0.55	0.50	0.41
A	a1	1.00	1.00	1.00	1.00	1.00	1.00	1.00	1.00	1.00	1.00
L	g1	0.46	0.48	0.52	0.48	0.60	0.45	0.44	0.36	0.57	0.55
	g2	0.36	0.36	0.32	0.40	0.29	0.38	0.46	0.52	0.26	0.36
	g3	0.18	0.15	0.16	0.12	0.11	0.17	0.10	0.11	0.18	0.09

Table 8. The harmonious super-matrix

Criteria		C				T		A	L		
	Sub-criteria	c1	c2	c3	c4	t1	t2	a1	g1	g2	g3
C	c1	0.07	0.07	0.07	0.07	0.07	0.07	0.08	0.07	0.07	0.07
	c2	0.07	0.07	0.07	0.07	0.08	0.07	0.08	0.07	0.08	0.08
	c3	0.06	0.06	0.07	0.06	0.06	0.06	0.06	0.06	0.06	0.06
	c4	0.08	0.08	0.08	0.08	0.08	0.08	0.08	0.08	0.08	0.08
T	t1	0.12	0.12	0.12	0.12	0.12	0.11	0.11	0.12	0.12	0.12
	t2	0.11	0.11	0.12	0.12	0.11	0.12	0.11	0.11	0.11	0.11
A	a1	0.23	0.23	0.23	0.23	0.23	0.23	0.23	0.23	0.23	0.23
L	g1	0.12	0.12	0.12	0.12	0.12	0.12	0.12	0.12	0.12	0.12
	g2	0.10	0.10	0.10	0.10	0.10	0.10	0.10	0.10	0.10	0.10
	g3	0.03	0.03	0.03	0.03	0.03	0.03	0.03	0.03	0.03	0.03

Table 9. Limiting the harmonious super-matrix

Criteria		C				T		A	L		
	Sub-criteria	c1	c2	c3	c4	t1	t2	a1	g1	g2	g3
C	c1	0.07	0.07	0.07	0.07	0.07	0.07	0.08	0.07	0.07	0.07
	c2	0.07	0.07	0.07	0.07	0.08	0.07	0.08	0.07	0.08	0.08
	c3	0.06	0.06	0.07	0.06	0.06	0.06	0.06	0.06	0.06	0.06
	c4	0.08	0.08	0.08	0.08	0.08	0.08	0.08	0.08	0.08	0.08
T	t1	0.12	0.12	0.12	0.12	0.12	0.11	0.11	0.12	0.12	0.12
	t2	0.11	0.11	0.12	0.12	0.11	0.12	0.11	0.11	0.11	0.11
A	a1	0.23	0.23	0.23	0.23	0.23	0.23	0.23	0.23	0.23	0.23
L	g1	0.12	0.12	0.12	0.12	0.12	0.12	0.12	0.12	0.12	0.12
	g2	0.10	0.10	0.10	0.10	0.10	0.10	0.10	0.10	0.10	0.10
	g3	0.03	0.03	0.03	0.03	0.03	0.03	0.03	0.03	0.03	0.03

Table 10. Influential Weights of the DANP

Criteria	Sub-criteria	Sub-Criteria Weight	Clusters Weight
C	c_1	0.0729	0.2876
	c_2	0.0735	0.0000
	c_3	0.0646	0.0000
	c_4	0.0766	0.0000
T	t_1	0.1212	0.2349
	t_2	0.1138	0.0000
A	a_1	0.2259	0.2259
L	g_1	0.1194	0.2516
	g_2	0.0992	0.0000
	g_3	0.0330	0.0000

3. Dataset Description

After obtaining the results of the DANP method, and determining the weight of each factor, we prepared the layers used. Moreover, elevation, slope, and stream layers are extracted from DEM with 10 resolutions in pixel size. The faults and lithology layer, prepared by the Geological Organization of Iran, was used with a scale of 1.100000. The layers of temperature, precipitation, and evaporation were obtained from the interpolation of the data by the Meteorological Organization. For the pedology layer, we used the pedology layer of the Natural Resources Organization (NRO). Finally, for the vegetation layer, we used the NDVI vegetation index applied to the Landsat images. The reference data were obtained by interpreting images from World Imagery and Google Earth, and the accuracy of the model using completeness, correctness, and quality indexed was calculated. Figure 6 shows the flowchart of the steps of the study.

Figure 3 shows a map of the criteria used in this study. Figure (7-a) shows the elevation map of the area, which ranges between 1,194 and 3,371 meters. Figure (7-b) shows the slope map of the area. Figure (7-c) represents the vegetation map of the area during the growing season. Figure (7-d) shows the precipitation map of the area. Figure (7-e) illustrates the evaporation map of the area. Figure (7-f) shows the average annual temperature map. Figure (7-g) shows the stone units of the study area. Figure (7-h) shows the pedology map. Figures (7-i) and (7-j) are the distance from the streams and faults, respectively, which are created using the Euclidean distance function.

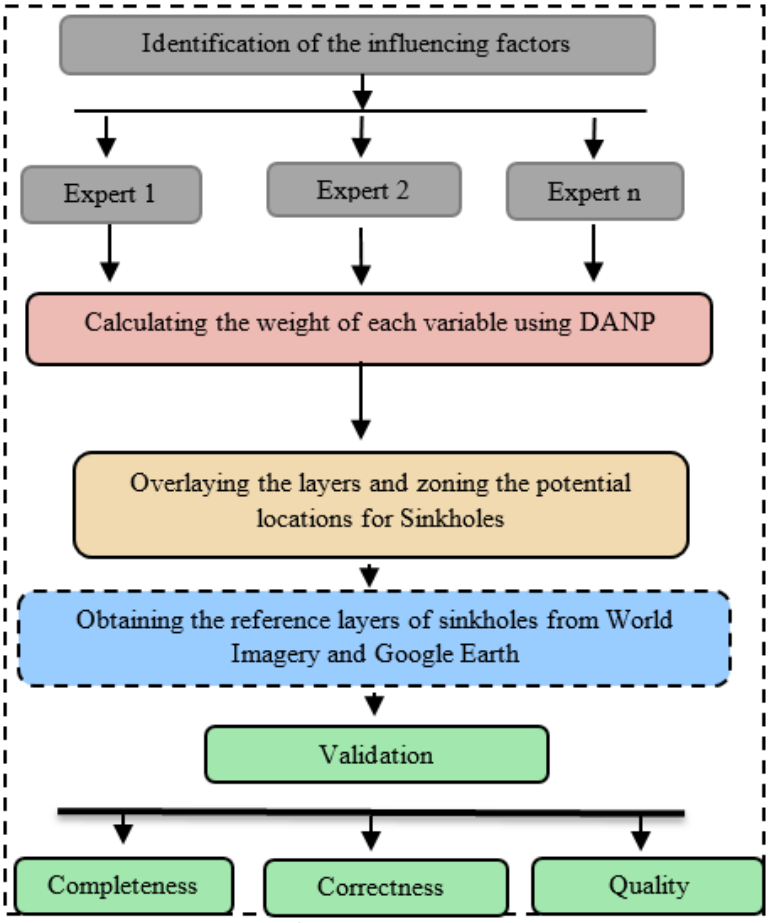

Figure 6. Study flowchart

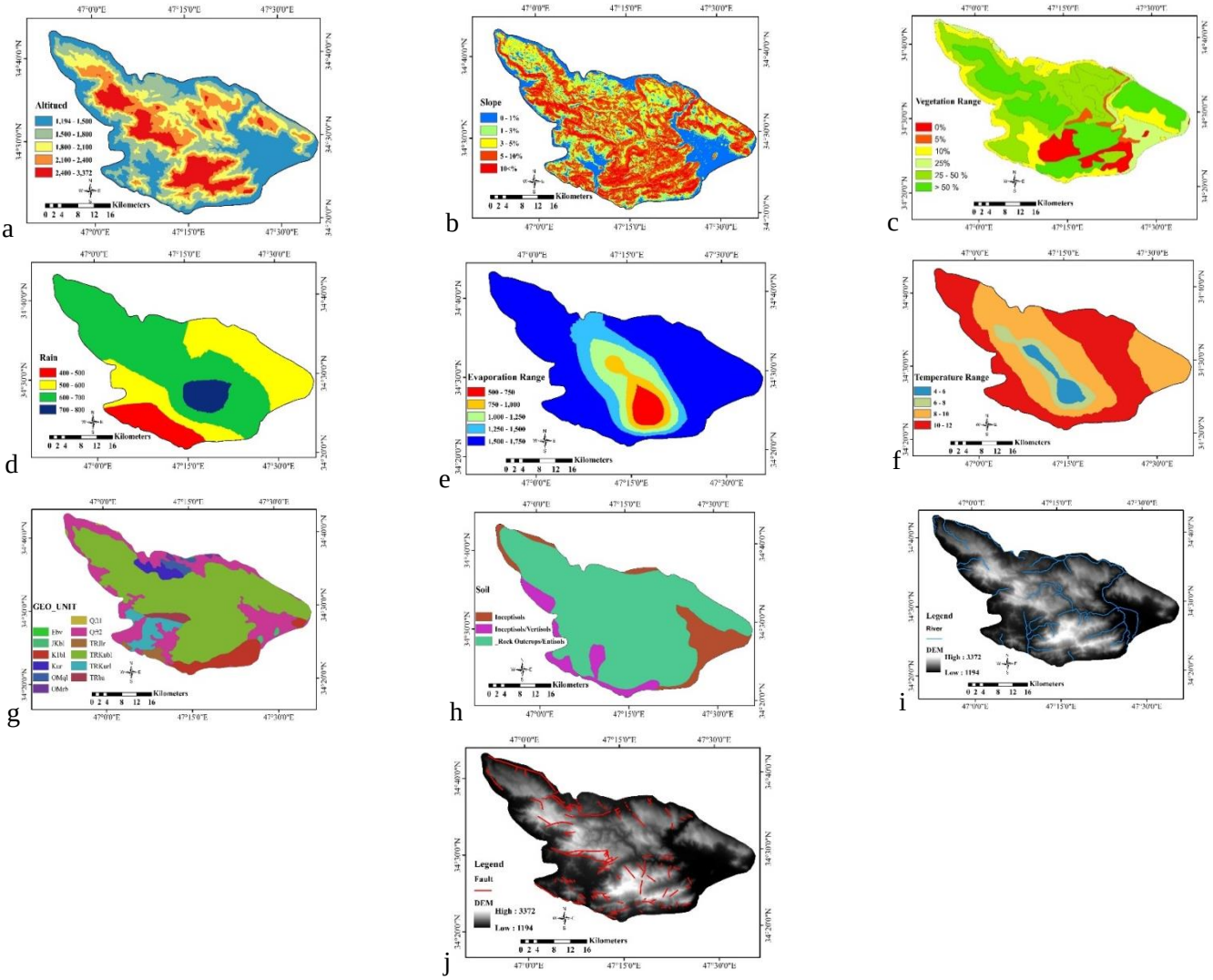

Figure 7. Criteria maps a) elevation; b) slope; c) vegetation; d) precipitation; e) evaporation; f) temperature; g) lithology; h) soil type; i) distance from streams; j) distance from faults

4. Experimental Results

In this study, three pixel-based indexes including completeness, correctness, and quality to quantitatively evaluate the results have been used. In order to use these indexes, the factors used in each index have to be introduced: **Completeness**: This index shows what percentage of the objects existing in the reference data as sinkholes are recognized correctly as sinkholes in the study. In addition, this index is defined as detection rate (Song & Haithcoat, 2005) or producer's accuracy (Foody, 2002). The objects that are related to other objects and are wrongly detected do not affect the value of this index. Therefore, the index is defined as in the following equation (Sohn & Dowman, 2007; Vayghan, Salmani, Ghasemkhani, Pradhan, & Alamri, 2020).

Completeness = (TP/TP+FN)*100 (14)

Correctness: This index is also referred to as s user's accuracy (Foody, 2002). It shows what percentage of the objects that have been detected as sinkholes in the results are the same as those in the reference data. The objects that were in the reference data but were not detected in the study do not affect the value of this index. This index can be defined as the following (Sohn & Dowman, 2007; Vayghan et al., 2020).

Correctness= (TP / FP+TP)*100 (15)

Quality: This index is a criterion to evaluate the results, which considers both the index of correctness and

completeness (Rutzinger, Rottensteiner, & Pfeifer, 2009). This index can be defined as the following (Sohn & Dowman, 2007; Vayghan et al., 2020).

Quality = (TP/TP+FP+FN) *100 (16)

In the above equations, true positive (TP) and true negative (TN) represent the pixels that are correctly detected as sinkholes and non-sinkholes, and false-negative (FN) represents the undetected sinkholes pixels. False-positive (FP)denotes the pixels that have been mistakenly detected as sinkholes (Vayghan et al., 2020).

Table 11 shows the results of the analytic network process and the relative weight of each of the factors influencing the karstification process and the formation of sinkholes.

Table 11. The relative weight of each parameter

Sub-criteria	Weight (%)	Sub-criteria	Weight (%)
Lithology	11.94	Soil type	9.92
Precipitation	7.29	Fault	3.3
Stream	7.35	Slope	11.38
Temperature	6.46	Evaporation	7.66
Elevation	12.12	Vegetation	22.59

Figure 8 shows an example of some sinkholes extracted by interpreting the World Imagery and Google Earth images.

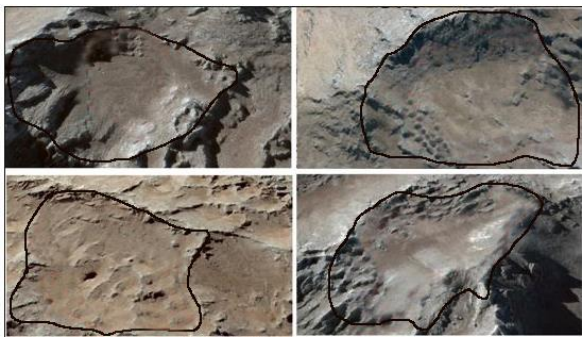

Figure 8. Examples of sinkholes using the interpretation of images of Google earth and world imagery

Figure 9 shows a map of potential areas for sinkhole formation using the criteria employed. Figure 10 shows a map of the sinkholes in the Bisotun-Parav mass obtained by interpreting the images from google earth and world imagery, along with a map showing the potential for sinkhole formation. With the aforementioned images, 46 sinkholes were detected in the study area.

Figure 9. Map of potential areas for sinkhole formation in the study area

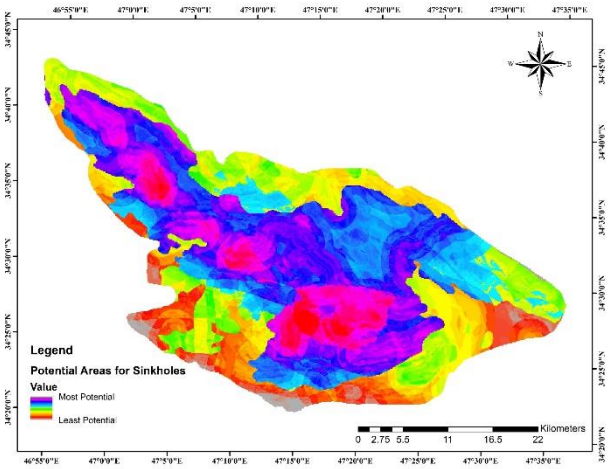

Figure 10. Reference sinkholes along with a map of sinkhole potential

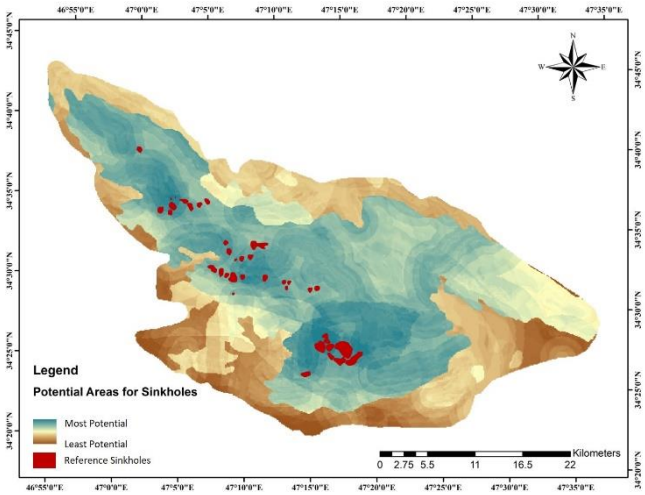

Table 12 presents the statistical parameters obtained from the study results, including the area of the reference sinkholes, which have been identified from the interpretation of high-resolution images. The area of the correctly detected sinkholes consists of the zones that have been correctly detected using the criteria employed. The table also shows the indexes used.

Table 12. Statistical parameters resulting from the study

The area of the reference sinkholes (meter)	The area of sinkholes correctly detected (meter)	Correctness	Completeness	Quality
12,017,241	9720417.97	98.73	79.86	79

5. Conclusions

A glance at table 2 shows that the highest relative weight in the karstification process and the formation of sinkholes is associated with the vegetation (22.59%) factor. Another important factor is the amount of elevation (12.12%). According to the result of the study conducted by Jonathan Launspach et al. (2013) during a master's thesis at the University of Northern Iowa entitled "Automated sinkhole extraction and morphological analysis in northeast Iowa using high-resolution LiDAR data", the main influential factor in controlling sinkholes is recharging groundwater. Thus it is possible by two pivotal factors, permeability, and lithology (Launspach, 2013). Moreover, water infiltration into the soil depends on factors such as soil texture and structure, vegetation, land slope, and most importantly, the dispersion of soil surface particles (Alizadeh, 1988). Furthermore, there is a direct relationship between vegetation and porosity. The growing amount of vegetation on the ground leads to increase infiltration by expanding numbers and size of seams and gaps in soils and geological formations. Also, vegetation reducing the velocity of surface flow, thus extending vegetation increases the permeability into the soil significantly.

Due to the specific tectonic and lithological conditions in the Parav-Bisotun area, there is a possibility for the development of dissolution and morphological processes in the surface and depth. Karstic processes are still going on with the current climatic conditions at altitudes above 2,500 (Maleki, 2001). The presence of thick, greatly pure limestone layers has provided suitable conditions for the development of karstic processes in the depths. Disruptions and disintegrations caused by fault activities can pave the way for orientating the dissolution processes in the depth and forming sinkholes incongruity with gaps (Jafarbeyglou, Moghimi, & Safari, 2012). There a direct relationship between elevation and precipitation. Furthermore, increased precipitation, especially in the form of snow, enhances the karstification process, which also explains the factors of altitude and temperature. The presence of streams helps to form sinkholes by washing limestone to reach the lower resistant rock. Also, fault activity results in the collapse of the loosened and decomposed area, causing the sinkhole to form. But the reason why the third most important factor in the formation of sinkholes is the lithology factor is that, to start with, the bedrock should have the ability to become karstic, then other factors help to enhance this process.

As shown in Table 12, the correctness of 98.73% indicates a very high efficacy in identifying potential areas for sinkholes. The lower completeness and quality shown in the table do not mean that the model performed poorly, as these indexes are based on the sinkholes in the reference data, but the proposed map shows the potential areas for sinkholes. Low completeness and quality have another reason too, which is the fact that according to the available data, the authors could not identify all the sinkholes in the area for reasons, such as the small size of some sinkholes that have not yet been fully developed. Also, as mentioned before, the map of potential areas for sinkhole formation shows areas that can be converted to sinkholes in the future and not just sinkholes that have been formed in the past and are currently there.

This study shows the success rate of the DANP method, just as other studies show the success rate of other methods. For example, the study by (Lee, Shin, Ko, & Chang, 2016), who installed a thermal camera on a drone, showed that the holes (which were dug by hand) were colder than their surroundings. They also indicated the classifiers convolutional neural network (CNN) and boosted random forest (BRF) perform better than other classifiers. Also, (Wu, Deng, & Chen, 2016)applied the contour tree method to LiDAR images. Their study showed that the use of this method is very effective in detecting sinkholes. Moreover, (Rajabi 2018)used LiDAR data to develop a semi-automated model in ArcMap to detect sinkholes and also to estimate geometric characteristics of sinkholes (e.g. depth, length, circularity, area, and volume). On the other hand, a method based on measurements from several instruments including field spectrometry, geophysical ground penetration radar (GPR), and a frequency-domain electromagnetic (FDEM) instrument developed for predicting by (Goldshleger et al. 2018)using mapping and monitoring methods based on active and passive remote-sensing means. For instance, (Qiu, Wu, & Chen, 2020) identified a sinkhole of large dimensions in Missouri using the analyses of digital terrain models (DTMs) and topography in GIS. Then, they analyzed the effective factors, ranked them, and prepared a sinkhole sensitivity map. Furthermore, (Todd & Ivey-Burden, 2017) considered five factors in the identification of sinkhole-prone areas, including bedrock type, distance from the fault, drainage class, river slope, and soil depth. They found that the bedrock type is the most important factor in the formation of sinkholes. Ultimately, they prepared the map of sinkhole-prone.

References

Alavi, M. (1994). Tectonics of the Zagros orogenic belt of Iran: new data and interpretations. Tectonophysics, 229(3-4), 211-238.

Ali, H., & Choi, J.-h. (2019). A review of underground pipeline leakage and sinkhole monitoring methods based on wireless sensor networking. Sustainability, 11(15), 4007.

Alizadeh, A. (1988). Principle of Applied Hydrology. Astane-Ghods Razavi, Mashhad. 519 p: Farsi.

Amiri, M., Mazaheri, H., & Nazaripoya, H. (2004). Causes and mechanism for occurrence of sinkholes in famenin-kaboudrahang plain.

Beck, B. F. (1984). Sinkhole development in south Georgia and Florida, USA, and the founding of the Florida Sinkhole Research Institute. Paper presented at the Third International Symposium on Land Subsidence.

Behniafar, A., Ghanbarzadeh, H., & Farzaneh, A. (2009). Geomorphic characteristics of akhlamad karst in north slops of bin aloud.

Chen, H., Oguchi, T., & Wu, P. (2018). Morphometric analysis of sinkholes using a semi-automatic approach in Zhijin County, China. Arabian Journal of Geosciences, 11(15), 1-14.

Chen, Z., Auler, A. S., Bakalowicz, M., Drew, D., Griger, F., Hartmann, J., . . . Stevanovic, Z. (2017). The World Karst Aquifer Mapping project: concept, mapping procedure and map of Europe. Hydrogeology Journal, 25(3), 771-785.

Chiu, W.-Y., Tzeng, G.-H., & Li, H.-L. (2013). A new hybrid MCDM model combining DANP with VIKOR to improve e-store business. Knowledge-Based Systems, 37, 48-61.

Doctor, D. H., & Young, J. A. (2013). An evaluation of automated GIS tools for delineating karst sinkholes and closed depressions from 1-meter lidar-derived digital elevation data.

Foody, G. M. (2002). Status of land cover classification accuracy assessment. Remote sensing of environment, 80(1), 185-201.

Ford, D., & Williams, P. D. (2013). Karst hydrogeology and geomorphology: John Wiley & Sons.

Ford, D. C., & Williams, P. W. (1989). Karst geomorphology and hydrology (Vol. 601): Unwin Hyman London.

García-Melón, M., Ferrís-Oñate, J., Aznar-Bellver, J., Aragonés-Beltrán, P., & Poveda-Bautista, R. (2008). Farmland appraisal based on the analytic network process. Journal of Global Optimization, 42(2), 143-155.

Gökkaya, E., Gutiérrez, F., Ferk, M., & Görüm, T. (2021). Sinkhole development in the Sivas gypsum karst, Turkey. Geomorphology, 107746.

Gunn, J. (2004). Encyclopedia of caves and karst science: Taylor & Francis.

Gutiérrez, F., Guerrero, J., & Lucha, P. (2008). A genetic classification of sinkholes illustrated from evaporite paleokarst exposures in Spain. Environmental Geology, 53(5), 993-1006.

Gutiérrez, F., Parise, M., De Waele, J., & Jourde, H. (2014). A review on natural and human-induced geohazards and impacts in karst. Earth-Science Reviews, 138, 61-88.

Harmon, R. S., Wicks, C. M., Ford, D. C., & White, W. B. (2006). Perspectives on karst geomorphology, hydrology, and geochemistry: a tribute volume to Derek C. Ford and William B. White (Vol. 404): Geological Society of America.

Harrison, R. W., Newell, W. L., Necdet, M., & Kuniansky, E. (2002). Karstification along an active fault zone in Cyprus. US Geological Survey Karst Interest Group Proceedings, Shepherdstown, West Virginia, 45-48.

Jafarbeyglou, M., Moghimi, E., & Safari, F. (2012). Evaluating morphotectonic karst sinks in Parav-Bistoun mass using DEM.

Jennings, J. N. (1985). Karst geomorphology. Basil Blackwell Inc. New York. 1985. 293.

Jia, L., Meng, Y., Li, L., & Yin, R. (2021). A multidisciplinary approach in cover-collapse sinkhole analyses in the mantle karst from Guangzhou City (SE China). Natural Hazards, 1-22.

Kheybari, S., Rezaie, F. M., & Farazmand, H. (2020). Analytic network process: An overview of applications. Applied mathematics and Computation, 367, 124780.

Khoshakhlagh, F., BAGHERI, S. S. S., & Safarrad, T. (2015). The Analysis of Severe Droughts Influences on Karst Springs Discharge in Kermanshah Province Case Study: Severe Drought of Year (1386-87).

Launspach, J. (2013). Automated sinkhole extraction and morphological analysis in northeast Iowa using high-resolution LiDAR data.

Lee, E. J., Shin, S. Y., Ko, B. C., & Chang, C. (2016). Early sinkhole detection using a drone-based thermal camera and image processing. Infrared Physics & Technology, 78, 223-232.

Maghsoudi, M., Karimi, H., Safari, F., & Charrahi, Z. (2010). Study of Karst Development Using Recession Coefficient, Spring Death Time and Chemical and Isotope Analysis in Parav-Bistoun Massif (Kermanshah Province-West of Iran). Physical Geography Research Quarterly, 41(69).

Maleki, A. (2001). Transformation of karst forms and its role in groundwater resources. PhD.

Milanovic, P. T. (1981). Karst hydrogeology: Water Resources Publications.

Mukherjee, A., & Zachos, L. (2012). GIS analysis of sinkhole distribution in Nixa, Missouri. Paper presented at the Geological Society of America Abstracts with Programs.

Obu, J., & Podobnikar, T. (2013). Algorithm for karst depression recognition using digital terrain models. Geodetski vestnik, 57(2), 260-270.

Plan, L., Decker, K., & Faber, R. (2003). Attributed Sinks-A GIS-Tool Quantifying Morphological Vulnerability Parameters in Karstic Catchment Areas. Paper presented at the EGS-AGU-EUG Joint Assembly.

Qiu, X., Wu, S.-S., & Chen, Y. (2020). Sinkhole susceptibility assessment based on morphological, imagery, and contextual attributes derived from gis and imagery data. Journal of Cave and Karst Studies, 82(1), 1-17.

Rahimi, M., & Alexander Jr, E. C. (2013). Locating sinkholes in LiDAR coverage of a glacio-fluvial karst, Winona County, MN.

Rosa, A. L., Pagli, C., Molli, G., Casu, F., Luca, C. D., Pieroni, A., & D'Amato Avanzi, G. (2018). Growth of a sinkhole in a seismic zone of the northern Apennines (Italy). Natural Hazards and Earth System Sciences, 18(9), 2355-2366.

Rosdi, M. A. H. M., Othman, A. N., Abdul, M. A. M. Z. Z., & Yusoff, Z. M. (2017). Sinkhole susceptibility hazard zones using gis and analytical hierarchical process (ahp): a case study of kuala lumpur and ampang jaya. International Archives of the Photogrammetry, Remote Sensing & Spatial Information Sciences, 42.

Rose, M. D., Federico, A., & Parise, M. (2004). Sinkhole genesis and evolution in Apulia, and their interrelations with the anthropogenic environment. Natural Hazards and Earth System Sciences, 4(5/6), 747-755.

Rutzinger, M., Rottensteiner, F., & Pfeifer, N. (2009). A comparison of evaluation techniques for building extraction from airborne laser scanning. IEEE Journal of selected topics in applied earth observations and remote sensing, 2(1), 11-20.

Saaty, T. L. (1999). Fundamentals of the analytic network process. Paper presented at the Proceedings of the 5th international symposium on the analytic hierarchy process.

Salvati, R., & Sasowsky, I. D. (2002). Development of collapse sinkholes in areas of groundwater discharge. Journal of Hydrology, 264(1-4), 1-11.

Sarvati, M. R., Rostami, M., Nosrati, K., & Ahmadi, M. (2014). Recognition the factors affecting the distribution and occurrence of Sinkholes in the region of Kermanshah Gazorkhani by using logistic regression.

Sohn, G., & Dowman, I. (2007). Data fusion of high-resolution satellite imagery and LiDAR data for automatic building extraction. ISPRS Journal of Photogrammetry and Remote Sensing, 62(1), 43-63.

Song, W., & Haithcoat, T. L. (2005). Development of comprehensive accuracy assessment indexes for building footprint extraction. IEEE Transactions on Geoscience and Remote Sensing, 43(2), 402-404.

Taheri, K., Gutiérrez, F., Mohseni, H., Raeisi, E., & Taheri, M. (2015). Sinkhole susceptibility mapping using the analytical hierarchy process (AHP) and magnitude–frequency relationships: A case study in Hamadan province, Iran. Geomorphology, 234, 64-79.

Tharp, T. M. (1999). Mechanics of upward propagation of cover-collapse sinkholes. Engineering geology, 52(1-2), 23-33.

Tihansky, A. B. (1999). Sinkholes, west-central Florida. Land subsidence in the United States: US geological survey circular, 1182, 121-140.

Todd, A. L., & Ivey-Burden, L. (2017). Using Readily Available Data and GIS to Map Sinkhole Risk in the Karst Counties of Virginia.

Van Schoor, M. (2002). Detection of sinkholes using 2D electrical resistivity imaging. Journal of Applied Geophysics, 50(4), 393-399.

Vayghan, S. S., Salmani, M., Ghasemkhani, N., Pradhan, B., & Alamri, A. (2020). Artificial intelligence techniques in extracting building and tree footprints using aerial imagery and LiDAR data. Geocarto International, 1-29.

Wadas, S. H., Tanner, D. C., Polom, U., & Krawczyk, C. M. (2017). Structural analysis of S-wave seismics around an urban sinkhole: evidence of enhanced dissolution in a strike-slip fault zone. Natural Hazards and Earth System Sciences, 17(12), 2335-2350.

Waltham, T., Waltham, A. C., Bell, F. G., & Culshaw, M. G. (2005). Sinkholes and subsidence: karst and cavernous rocks in engineering and construction: Springer Science & Business Media.

White, R. (1998). Cities and cellular automata. Discrete dynamics in Nature and Society, 2(2), 111-125.

Wu, Q., Deng, C., & Chen, Z. (2016). Automated delineation of karst sinkholes from LiDAR-derived digital elevation models. Geomorphology, 266, 1-10.

Zebardast, E. (2010). The application of analytic network process (ANP) in urban and regional planning. Honar-Ha-Ye-Ziba: Memary Va Shahrsazi, 2(41), 79-90.

Zeng, Y., & Zhou, W. (2019). Sinkhole remedial alternative analysis on karst lands. Carbonates and Evaporites, 34(1), 159-173.

Zhu, J., Taylor, T. P., Currens, J. C., & Crawford, M. M. (2014). Improved karst sinkhole mapping in kentucky using lidar techniques: a pilot study in floyds fork watershed. Journal of Cave & Karst Studies, 76(3).